Hexadecane ($C_{16}H_{34}$) + 1-Hexadecanol ($C_{16}H_{33}OH$) Binary System: Crystal Structures of the Components and Experimental Phase Diagram. Application to Thermal Protection of Liquids

Valérie Métivaud,[†] Adeline Lefèvre,[†] Lourdes Ventolà,[†] Philippe Négrier,[‡] Evelyn Moreno,[†] Teresa Calvet,[†] Denise Mondieig,[‡] and Miquel Angel Cuevas-Diarte*[,†]

Departament de Cristal.lografia, Mineralogía i Dipòsits Minerals, Facultat de Geología, Universitat de Barcelona, C/Martí i Franquès s/n, 08028 Barcelona, Spain, and Centre de Physique Moléculaire Optique et Hertzienne, UMR 5798 au CNRS, Université Bordeaux I, 351 cours de la Libération, 33405 Talence Cedex, France

Received January 20, 2005. Revised Manuscript Received March 18, 2005

The experimental temperature−composition phase diagram of the binary system between hexadecane ($C_{16}H_{34}$) and 1-hexadecanol ($C_{16}H_{33}OH$) has been established by combining thermal analysis and powder X-ray diffraction (XRD). Beforehand, crystal structures of the solid ordered phases of the components involved were determined from XRD data. Hexadecane displays a triclinic form T_p belonging to the space group $P\bar{1}$, with $Z = 1$. The unit cell dimensions are $a = 4.269$ Å, $b = 4.811$ Å, $c = 22.34$ Å, $\alpha = 84.54°$, $\beta = 67.43°$, and $\gamma = 73.00°$. 1-Hexadecanol displays a monoclinic form γ belonging to the space group $A2/a$ with $Z = 8$. The unit cell dimensions are $a = 8.980$ Å, $b = 4.939$ Å, $c = 87.91$ Å, and $\beta = 122.63°$. The phase diagram between both components is characterized by two invariants, a eutectic (located at $T = 289.5$ K) and a metatectic (located at $T = 318.8$ K). The miscibility in the solid state is very restricted, limited to the regions rich in $C_{16}H_{34}$ and $C_{16}H_{33}OH$. Resulting alloys have led to the design of a double-wall glass for the thermal protection of liquid products between 13 and 18 °C, effective for 4.5 h in an external environmental temperature of 24 °C.

Introduction

This work is part of a general study on organic syncrystallization, undertaken a few years ago within our research group and the REALM collaborating laboratories. [The REALM (Réseau Européen sur les ALiages Moléculaires) gathers four Research Groups of the Spanish Universities of Barcelona and Polytechnic of Catalonia, the French University of Bordeaux I, and the Dutch University of Utrecht.] During the past decade, two families have been studied extensively from structural and thermodynamic points of view: *n*-alkanes (C_nH_{2n+2}) and 1-alkanols ($C_nH_{2n+1}OH$).

Normal alkanes are the main constituents of petroleum waxes and the knowledge of their mixture properties is of great interest. Furthermore, they can be used as models for the description of more complex substances, such as polymers and biomembranes. Within the REALM, no less than 19 binary systems involving odd and even *n*-alkanes with 8 to 28 carbon atoms have been studied.[1−6] Their experimental phase diagrams have pointed out that no continuous miscibility is observed at "low temperature" (i.e., in the solid-ordered phase domain), even if the crystal symmetries of the pure components are the same (which is the case for odd−odd and even−even alkane systems). Instead, several crystalline forms which are metastable for the pure components are stabilized by mixing. These forms have been identified as those observed in long alkanes from $C_{25}H_{52}$.[7]

1-Alkanols are among the simplest of the substituted hydrocarbons. A single −OH group replaces a hydrogen atom at one end of the aliphatic chain. Pure alkanols from 1-undecanol to 1-eicosanol as well as 10 binary systems (involving components with 15−20 carbon atoms) have been studied within our research group,[8−11] and as for *n*-alkane systems, results indicate that in some cases (especially in the even−even systems), the mixing stabilizes forms which are only metastable for the pure components. As an example, for even−even systems between isostructural components, no continuous miscibility is observed, the mixing stabilizing at "low temperature" a form stable in odd alkanols.

* To whom correspondence should be addressed. Phone: (34)934021350. Fax: (34)934021340. E-mail. macuevasdiarte@ub.edu.
‡ Université Bordeaux I.
† Universitat de Barcelona.

(1) Rajabalee, F.; Espeau, P.; Haget, Y. *Mol. Cryst. Liq. Cryst.* **1995**, *269*, 165.
(2) Métivaud, V.; Rajabalee, F.; Cuevas-Diarte, M. A.; Calvet, T.; Mondieig, D.; Haget, Y. *An. Quim. Int. Ed.* **1998**, *94* (6), 396.
(3) Métivaud, V.; Rajabalee, F.; Cuevas-Diarte, M. A.; Mondieig, D.; Haget, Y. *Chem. Mater.* **1999**, *11* (1), 117.
(4) Rajabalee, F.; Métivaud, V.; Mondieig, D.; Oonk, H. A. J.; Haget, Y. *Chem. Mater.* **1999**, *11* (10), 2788.
(5) Rajabalee, F.; Métivaud, V.; Mondieig, D.; Oonk, H. A. J.; Haget, Y. *Helv. Chim. Acta* **1999**, *82* (11), 1916.
(6) Mondieig, D.; Rajabalee, F.; Métivaud, V.; Oonk, H. A. J.; Cuevas-Diarte, M. A. *Chem. Mater.* **2004**, *16* (5), 786.
(7) Rajabalee, F.; Métivaud, V.; Mondieig, D.; Haget, Y.; Cuevas-Diarte, M. A. *J. Mater. Res.* **1999**, *14* (6), 2644.
(8) Ventolà, L. Ph. D. European Thesis, University of Barcelona, Spain, 2001.
(9) Ramírez, M. Ph. D. European Thesis, University of Barcelona, Spain, 2002.
(10) Ventolà, L.; Calvet, T.; Cuevas-Diarte, M. A.; Mondieig, D.; Oonk, H. A. *J. Phys. Chem. Chem. Phys.* **2002**, *4*, 1953.
(11) Ventolà, L.; Calvet, T.; Cuevas-Diarte, M. A.; Ramírez, M.; Oonk, H. A. J.; Mondieig, D.; Négrier, P. *Phys. Chem. Chem. Phys.* **2004**, *6*, 1786.

10.1021/cm050130c CCC: $30.25
Published on Web 05/17/2005

Be that as it may, for both organic families, the global miscibility is quite extensive.

In addition, from a practical point of view, these kinds of mixed substances have proved their efficiency as MAPCM (molecular alloy phase change materials) for industrial applications in the fields of energy storage and thermal protection.[12−16] Many applications, at different temperature levels (approximately from −11 to 90 °C), have been developed lately or are currently in progress within the REALM. Among them, we can mention the design of containers for the thermal protection of foodstuffs[17−19] and biomedical and pharmaceutical products,[20] as well as the development of systems for the thermal protection of electronic devices[21] and the heating and insulation of buildings.[22,23]

Subsequently, we have decided to extend the study to the binary systems between *n*-alkanes and 1-alkanols, to investigate the solid-state miscibility and application potentialities of the resulting mixed substances. Many experimental and thermodynamic studies based on the solid−liquid equilibria of binary systems formed by even *n*-alkanes (from octane to hexadecane) and 1-alkanols (from 1-butanol to 1-eicosanol) have already been published.[24−32] Most of them have been carried out within the same research group of the Institute of Physical Chemistry of the Polish academy of sciences. In all cases, the authors have pointed out a total immiscibility in the solid phase between the two components, which means that they form a perfect eutectic. However, phase diagrams were only determined by means of calorimetric techniques and were not supported by any other kind of experiments, such as crystallographic or spectroscopic ones. That means the nature of the encountered phases has not really been confirmed.

The present paper deals with the experimental determination of the equilibrium phase diagram between two molecules with the same chain length: hexadecane ($C_{16}H_{34}$) and 1-hexadecanol ($C_{16}H_{33}OH$). These components will be hereafter denoted by C_{16} and $C_{16}OH$, respectively. To our knowledge, the solid−liquid phase diagram of this binary system has been reported only once in the literature.[29] Beforehand, structural and thermodynamic behaviors of both components will be discussed. An application relative to the design of a double-wall glass capable of maintaining the temperature of a liquid in a predetermined range for several hours is also presented.

Experimental Section

Materials. *n*-Hexadecane and 1-hexadecanol were purchased from Acros Organics and Fluka, respectively, with certified purity grades of 99%. Binary mixed samples were prepared according to the melting−quenching method: components were weighed in the desired proportions, melted together, mixed thoroughly to obtain an entirely homogeneous sample and then quenched into liquid nitrogen. To reduce heterogeneity and stability problems, which have been observed previously in mixed samples of alkanes[33] and alkanols,[34] analyses were systematically performed under the same experimental conditions, soon afterward the quenching.

Calorimetric Measurements. They were carried out using a Perkin-Elmer DSC7 differential scanning calorimeter (DSC) operating in the liquid nitrogen subambient mode. The calibration was made with substances of known transition temperatures and enthalpies (indium and *n*-decane). Thermo-energetic parameters were obtained from four independent experiments performed on (4.0 ± 0.1) mg samples with a scanning speed of 2 K·min^{-1}. The different transition temperatures were determined from the DSC curves by using the shape factor method.[35,36] The random part of the uncertainties was estimated using the Student's method with 95% threshold of reliability. The systematic part was estimated to ±0.2 K for temperatures and 2% for enthalpies.

Powder X-ray Diffraction Analyses. Isothermal crystallographic measurements were performed using the following: (a) a Siemens D500 vertical powder diffractometer, which works in the reflection mode with a Bragg−Brentano geometry, using Cu Kα radiation and a secondary monochromator. Diffraction patterns were recorded by means of an Anton PAAR TTK system. Data were collected in the angular range $1.5° \leq 2\theta \leq 60°$ with a 0.025° 2θ step and 3 s interval time. (b) An Inel CPS 120 diffractometer, equipped with a 600 series Cryostream cryostat from Oxford Cryosystems operating with liquid nitrogen. The detector, set up in a Debye−Scherrer geometry (transmission mode) and consisting of 4096 channels, enables a simultaneous recording of the profile over a 2θ range between 4 and 120° (angular step of 0.029° in 2θ). Monochromatic Cu $K\alpha_1$ radiation ($\lambda = 1.5406$ Å) was selected with the use of an asymmetric focusing incident-beam curved quartz

(12) Haget, Y.; Mondieig, D.; Cuevas-Diarte, M. A. U.S. Patent 6:136-217, 1999.
(13) Haget, Y.; Mondieig, D.; Cuevas-Diarte, M. A. European Patent EPO 548 334 B1, 1999.
(14) Mondieig, D.; Haget, Y.; Labrador, M.; Cuevas-Diarte, M. A.; Van der Linde, P. R.; Oonk, H. A. J. *J. Mater. Res. Bull.* **1991**, *26*, 1091.
(15) Espeau, P.; Roblès, L.; Cuevas-Diarte, M. A.; Mondieig, D.; Haget, Y. *J. Mater. Res. Bull.* **1996**, *31* (10), 1219.
(16) Mondieig, D.; Marbeuf, A.; Robles, L.; Espeau, P.; Poirier, B.; Haget, Y.; Calvet-Pallas, T.; Cuevas-Diarte, M. A. *High Temp.-High Pressures* **1997**, *29*, 385.
(17) Espeau, P.; Mondieig, D.; Haget, Y.; Cuevas-Diarte, M. A. *Packag. Technol. Sci.* **1997**, *10*, 253.
(18) Arjona, F.; Calvet, T., Cuevas-Diarte, M. A.; Métivaud, V.; Mondieig, D. *Bol. Soc. Esp. Cerám. Vidrio* **2000**, *19* (4), 548.
(19) Ventola, L.; Calvet, T., Cuevas-Diarte, M. A.; Métivaud, V.; Mondieig, D.; Oonk, H. A. *J. Mater. Res. Innovat.* **2002**, *6*, 284.
(20) Mondieig, D.; Rajabalee, F.; Laprie, A.; Oonk, H. A. J., Calvet, T.; Cuevas-Diarte, M. A. *Transfus. Apher. Sci.* **2003**, *28*, 143.
(21) Grignon, R.; Girardet, C.; Haget, Y. *XXèmes Journées d'Etudes des Equilibres entre Phases*, Bordeaux, France, 23−24 march 1994; p 113.
(22) Cuevas-Diarte, M. A.; Calvet, T.; Aguilar, M.; Arjona, F.; Mondieig, D. Technical report, Barcelona, 1999.
(23) Métivaud, V.; Ventola, L.; Calvet, T.; Cuevas-Diarte, M. A.; Mondieig, D. *IEA, ECES IA, Annex 17*, 6th workshop, Arvika, Sweden, 8−9 june 2004.
(24) Plesnar, Z.; Gierycz, P.; Bylicki, A. *Thermochim. Acta* **1988**, *128*, 93.
(25) Plesnar, Z.; Gierycz, P. *Pol. J. Chem.* **1989**, *150*, 101.
(26) Plesnar, Z.; Gierycz, P.; Gregorowicz, J.; Bylicki, A. *Thermochim. Acta* **1989**, *150*, 101.
(27) Plesnar, Z.; Gierycz, P.; Bylicki, A. *J. Chem. Thermodyn.* **1990**, *22*, 393.
(28) Plesnar, Z.; Gierycz, P.; Bylicki, A. *J. Chem. Thermodyn.* **1990**, *22*, 403.
(29) Plesnar, Z.; Bylicki, A. *J. Chem. Thermodyn.* **1993**, *25*, 1301.
(30) Plesnar, Z.; Bylicki, A. *J. Chem. Thermodyn.* **1993**, *25*, 1447.
(31) Domańska, U.; Roliñska, J. *Fluid Phase Equilib.* **1993**, *86*, 233.
(32) González, J. A.; Garcia de la Fuente, I.; Cobos, J. C.; Domańska, U. *Fluid Phase Equilib.* **1994**, *94*, 167.
(33) Mondieig, D.; Métivaud, V.; Oonk, H. A. J.; Cuevas-Diarte, M. A. *Chem. Mater.* **2003**, *15* (13), 2552.
(34) Ventolà, L.; Calvet, T.; Cuevas-Diarte, M. A.; Solans, X.; Mondieig, D.; Négrier, P.; van Miltenburg, J. C. *Phys. Chem. Chem. Phys.* **2003**, *5*, 947.
(35) Courchinoux, R.; Chanh, N. B.; Haget, Y.; Tauler, E.; Cuevas-Diarte, M. A. *Thermochim. Acta* **1988**, *128*, 45.
(36) Courchinoux, R.; Chanh, N. B.; Haget, Y.; Calvet, T.; Estop, E.; Cuevas-Diarte, M. A. *J. Chim. Phys.* **1989**, *86* (3), 561.

monochromator. The generator power was set to 1.0 kW (40 kV and 25 mA). Samples were introduced into 0.5 mm diameter Lindemann glass capillaries and were rotated perpendicularly to the X-ray beam during data collection. Data acquisition time was 5 h. External calibration using the cubic Na2Ca3Al2F14 phase was performed for channels to be converted into 2θ degrees by means of cubic spline fittings.[37] PEAKOC application from DIFFRACTINEL software was used for the calibration and the peak position determination after pseudo-Voigt fittings.

Diffraction measurements were also carried out versus continuous temperature variations with a Guinier-Simon camera (GS), working in the transmission mode with Cu $K\alpha_1$ radiation. Samples were introduced into 0.5 mm diameter Lindemann glass capillaries and then mounted perpendicular to the X-ray radiation beam. The continuous evolution of the X-ray patterns was recorded on photographic films, moved perpendicularly to the beam at a constant rate of 1 mm·h^{-1}.

Crystal Structure Determination. Structures and cell parameters of both components at 273 K were determined from Inel experimental X-ray diffraction data using the MATERIALS STUDIO software.[38] A Pawley profile-fitting procedure[39] was first used. For a given space group, the latter provides refinements of the cell and peak profile parameters, as well as those of the background, peak asymmetry, and zero shift. Afterward, both molecules were drawn in a 3D worksheet and minimized in energy, using geometry optimization by a COMPASS force field,[40] in order to obtain relevant values of distances, angles, and dihedral angles for the various bonds. The molecules were then set as rigid bodies, with the exception, in the case of $C_{16}OH$, of the dihedral angle of the alcohol group, let free to allow the good establishment of the hydrogen bonds. Each rigid body was introduced in its respective cell, whose dimensions have been determined previously. The whole entity was moved in the cells, according to the six (for C_{16}) or seven (for $C_{16}OH$) degrees of freedom (i.e., the three translations, the three rotations, and the dihedral angle of the −OH group), using a Monte Carlo simulation.[41] Several cycles were performed to obtain the best agreement between experimental and calculated X-ray diffraction patterns. The final structures were obtained after alternating Rietveld refinement[42] and geometry optimization by energy minimization. In addition to the parameters previously refined by the Pawley procedure, the Rietveld procedure includes the refinement of the translations, rotations, and dihedral angle of the molecules, as well as isotropic temperature factors and preferred orientations.

Cell parameters of the other encountered form (i.e., the rotator form of 1-hexadecanol) were refined from diffraction data with the Fullprof software using a profile matching option.[43]

Results and Discussion

Pure Component Properties. *n-Hexadecane.* The polymorphism of C_{16}, which has already been studied in our research group,[44] is as follows: $T_p \rightarrow$ Liquid.

Table 1. Melting Temperature and Enthalpy of C_{16}

	$T_p \rightarrow$ Liquid	
C_n	T_m (K)	ΔH_m (kJ/mol)
C_{16}	290.4 ± 0.6	53.0 ± 1.6

Table 2. Cell Parameters of C_{16} in the T_p Form ($P\bar{1}$, Z=1), Determined at T = 273 K

form	*a* (Å)	*b* (Å)	*c* (Å)	α (°)	*β* (°)	*γ* (°)
T_p	4.269(2)	4.811(3)	22.34(1)	84.54 (4)	67.43 (6)	73.00(2)

Melting temperature (T_m) and enthalpy (ΔH_m) are reported in Table 1.

The form T_p is triclinic with space group $P\bar{1}$ ($Z = 1$). The subscript "p" stands for "pair", the French word for "even". This crystalline form is observed in all even alkanes with chain lengths ranging from 6 to 24 carbon atoms.[44,45]

Only a few studies based on the crystal structure determination of *n*-alkanes have been published yet. Among even alkanes crystallizing in the triclinic system, we can mention the works of Norman et al.,[46] Mathisen et al.,[47] and Nyburg et al.[48] relative to hexane (C_6H_{14}), octane (C_8H_{18}), and octadecane ($C_{18}H_{38}$), respectively. To our knowledge, the hexadecane crystal structure has never been reported in the literature. However, Nyburg et al.[49] have suggested that with knowledge of the structure of a given *n*-alkane ($n = 18$ in the present case), the unit-cell dimensions and crystal structures of all other isostructural components belonging to the same family can be reliably predicted. These latter predictions are based on the assumption that the carbon chain (linear zigzag) preserves its orientation with respect to the crystallographic axes for each member of the isostructural series. Thus, if one chooses the longest cell dimension (generally *c*) to lie as close as possible to the molecular axis, it seems reliable to assume that the cell parameters *a*, *b*, and γ will not change significantly within the family. Cell parameters of *n*-hexadecane, as determined from our own study at $T = 273$ K, are given in Table 2. They are in quite good agreement with those predicted by Nyburg et al. Comparison between experimental and calculated XRD patterns of the T_p form after final Rietveld refinement is shown in Figure 1. The final agreement factors are $R_{wp} = 6.58\%$ and $R_p = 4.29\%$.

The molecular structure and intermolecular packing as viewed along the *c* and *b* axes are shown in Figures 2 and 3, respectively. The molecules display an all-trans conformation. The center of symmetry at the molecular midpoint lies between the eighth and ninth carbon atoms. Molecules are packed parallel to each other in a direction almost, but not exactly, parallel to the *c*-axis. The planes containing the carbon atoms are also parallel to each other. The length of the alkyl chain is 20.98 Å and the tilt angle is 19.07°. The mean carbon−carbon and carbon−hydrogen distances are

(37) Evain, M.; Deniard, P.; Jouanneaux, A.; Brec, R. *J. Appl. Crystallogr.* **1993**, *26* (4), 563.
(38) MS Modeling (Materials Studio) 3.0, http://www.accelrys.com/mstudio/ms_modeling.
(39) Pawley, G. S. *J. Appl. Crystallogr.* **1981**, *14*, 357.
(40) Sun, H. *J. Phys. Chem. B* **1998**, *102*, 7338.
(41) Harris, K. D. M.; Tremayne, M. *Chem. Mater.* **1996**, *8*, 2554.
(42) Rietveld, H. M. *J. Appl. Crystallogr.* **1969**, *2*, 65.
(43) Rodriguez-Carvajal, J. *FULLPROF: a program for Rietveld refinement and pattern matching* analyses; Abstracts of the satellite meeting on powder diffraction, XVth congress of the International Union of Crystallography, Toulouse, France, 1990; p 117.
(44) Espeau, P.; Roblès, L.; Mondieig, D.; Haget, Y.; Cuevas-Diarte, M. A.; Oonk, H. A. J. *J. Chim. Phys.* **1996**, *93*, 1217.
(45) Roblès, L.; Mondieig, D.; Haget, Y.; Cuevas-Diarte, M. A. *J. Chim. Phys.* **1998**, *95*, 92.
(46) Norman, N.; Mathisen, H. *Acta Chem. Scand.* **1961**, *15*, 1755.
(47) Mathisen, H.; Norman, N.; Pedersen, B. F. *Acta Chem. Scand.* **1967**, *21* (1), 127.
(48) Nyburg, S. C.; Lüth, H. *Acta Crystallogr.* **1972**, *B28*, 2992.
(49) Nyburg, S. C.; Potworowski, J. A. *Acta Crystallogr.* **1973**, *B29*, 347.

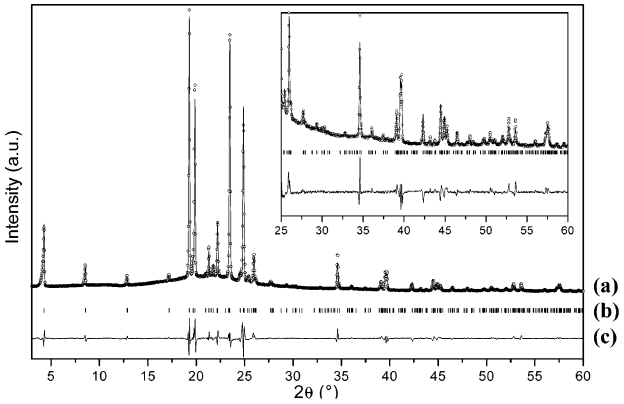

Figure 1. XRD patterns of C_{16} in the triclinic T_p form in the range $3° \leq 2\theta \leq 60°$. (a) Experimental (○) and calculated (−) diffraction patterns. (b) Position of calculated reflections. (c) Difference between experimental and calculated intensities.

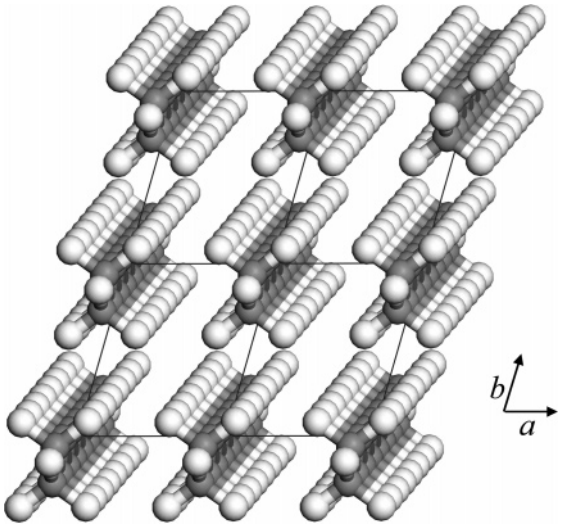

Figure 2. C_{16}: projection of the cell content along the *c*-axis.

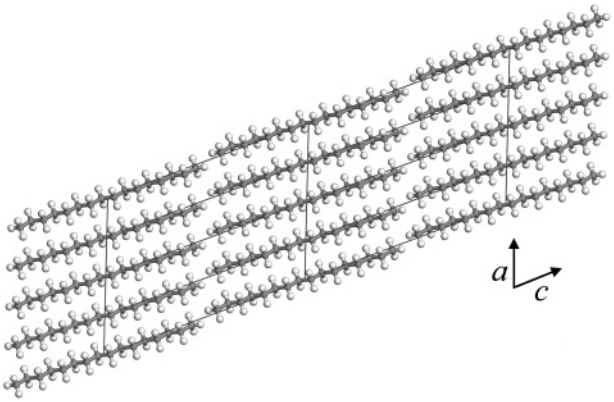

Figure 3. C_{16}: projection of the cell content along the *b*-axis.

1.532 Å and 1.104 Å, respectively, while the mean carbon−carbon−carbon, hydrogen−carbon−hydrogen, and carbon−carbon−hydrogen bond angles are 113.12°, 106.91°, and 109.42°, respectively. These values of C−C and C−C−C bond lengths and angles obtained after geometry minimization by means of COMPASS force field are in agreement with those published previously for the triclinic forms of hexane and octane,[46,47] the orthorhombic form of pentane (C_5H_{12}),[50] as well as the monoclinic and orthorhombic forms of hexatriacontone ($C_{36}H_{74}$).[51,52] The shortest intermolecular nonbonded contacts are all between hydrogen atoms. The mean closest H−H distance between adjacent chains is 2.49 Å.

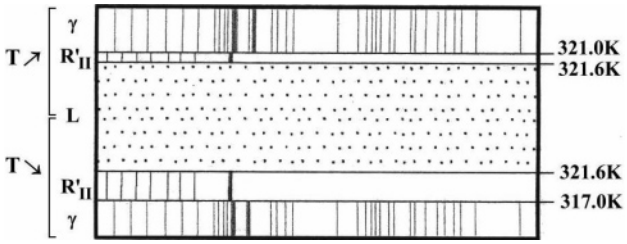

Figure 4. Schematization of the Guinier−Simon photograph of $C_{16}OH$.

Table 3. Cell Parameters of $C_{16}OH$ in the γ-Form ($A2/a$, $Z = 8$), and in the R'_{II} Form ($R\bar{3}m$, $Z = 6$), Determined at $T = 273$ K and $T = 319.4$ K, Respectively

form	*a* (Å)	*b* (Å)	*c* (Å)	α (°)	*β* (°)	*γ* (°)
γ	8.980(5)	4.939(3)	87.91(4)	90	122.63(3)	90
R'_{II}	4.905(4)	4.905(4)	133.3(3)	90	90	120

1-Hexadecanol. X-ray powder diffraction analyses versus continuous temperature have pointed out the presence of two different forms before melting (Figure 4), leading to the following polymorphic sequence: $\gamma \rightarrow R'_{II} \rightarrow$ Liquid.

To our knowledge, the complete crystal structure of the ordered *γ*-form, determined by single-crystal X-ray diffractometry, was reported only once in the literature in 1960.[53] This form was described as monoclinic, with space group *A*2/*a* and eight molecules in the unit cell. It is isostructural to those observed in $C_{18}H_{37}OH$ and $C_{20}H_{41}OH$.[54] Before melting, it transforms to a disordered form, reported as a hexagonal phase similar to the R_{II} phase of *n*-alkanes.[55] However, since no isostructural relationship between alkane and alkanol rotator phases has been yet established, we have opted for the notation R'_{II}.

Cell parameters of both phases were determined from X-ray diffraction patterns recorded at 273 and 319.4 K. Results, which are given in Table 3, are in good agreement with those published by Abrahamsson et al.[53] and Frede et al.[55] Experimental and calculated XRD patterns of the *γ*-form obtained after final Rietveld refinement at 273 K are given in Figure 5. The final agreement factors are $R_{wp} = 3.59\%$ and $R_p = 2.75\%$.

Molecular arrangements, as viewed along the *b* and *a* axes, are shown in Figures 6 and 7, respectively. The molecules are packed in bimolecular layers quasi-parallel to the (001) plane, with the hydrocarbon chains arranged according to the orthorhombic subcell. The length of the alkyl chain is 21.92 Å and the tilt angle is 34.26°. The molecules are linked together by infinite chains of hydrogen bonds along the *a* axis. All C−C bonds of the alkyl chain show a zigzag (trans) conformation with, however, a small deviation from the ideal

(50) Norman, N.; Mathisen, H. *Acta Chem. Scand.* **1964**, *18* (2), 353.
(51) Shearer, H. M. M.; Vand, V. *Acta Crystallogr.* **1956**, *9*, 379.
(52) Teare, P. W. *Acta Crystallogr.* **1959**, *12*, 294.
(53) Abrahamsson, S.; Larsson, G.; von Sydow, E. *Acta Crystallogr.* **1960**, *13*, 770.
(54) Ventolà, L.; Ramírez, M.; Calvet, T.; Solans, X.; Cuevas-Diarte, M. A.; Négrier, P.; Mondieig, D.; van Miltenburg, J. C.; Oonk, H. A. J. *Chem. Mater.* **2002**, *14*, 508.
(55) Frede, E.; Precht, D. *Kieler Milchw. Forsch.* **1974**, *26*, 325.

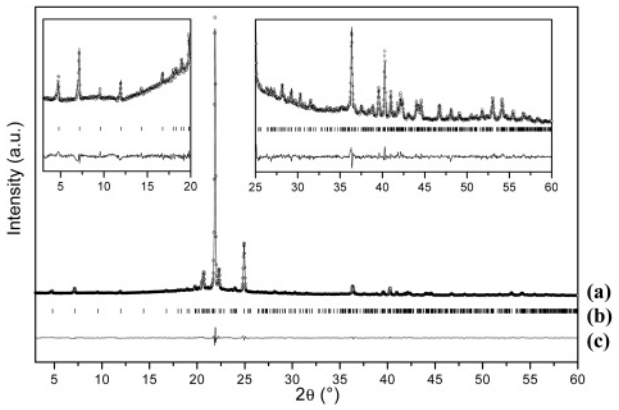

Figure 5. XRD patterns of $C_{16}OH$ in the monoclinic γ-form in the range $3° \leq 2\theta \leq 60°$. (a) Experimental (○) and calculated (−) diffraction patterns. (b) Position of calculated reflections. (c) Difference between experimental and calculated intensities.

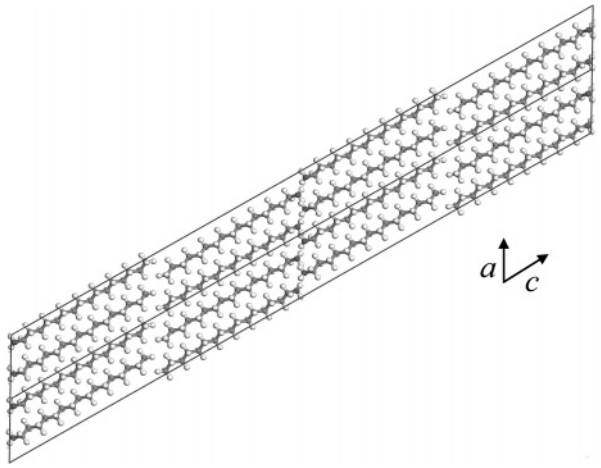

Figure 6. γ -form of $C_{16}OH$: projection of the cell content along the *b*-axis.

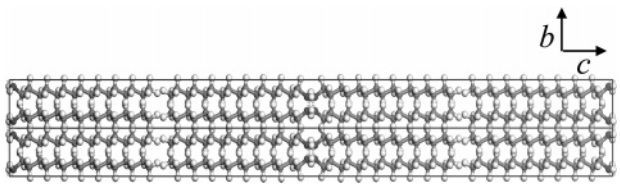

Figure 7. γ -form of $C_{16}OH$: projection of the cell content along the *a*-axis.

Table 4. γ-Form of $C_{16}OH$: Mean Intramolecular Bond Lengths and Angles

C−C (Å)	C−H (Å)	C−O (Å)	O−H (Å)
1.529	1.102	1.421	0.961
C−C−C (°)	**H−C−H (°)**	**C−C−H (°)**	**O−C−C (°)**
112.92	106.81	109.42	111.96

value (180°) in the C−C bonds close to the hydrogen ones: the C11−C12−C13−C14 [178.63°], C12−C13−C14−C15 [178.46°], C13−C14−C15−C16 [179.11°], and C14−C15−C16−O [167.32°] torsion angles deviate significantly from the ideal 180°, due to the steric hindrance produced by the hydrogen bonds. The different mean intramolecular bond lengths and angles are given in Table 4.

These values are in total agreement with those found for C_{16}, but are somewhat different from those published by Abrahamsson et al. for that same $C_{16}OH$ molecule. These authors have reported longer carbon−carbon and carbon−oxygen distances (1.55 Å and 1.44 Å, respectively) and smaller carbon−carbon−carbon and oxygen−carbon−carbon angles (110.72° and 109.18°, respectively).

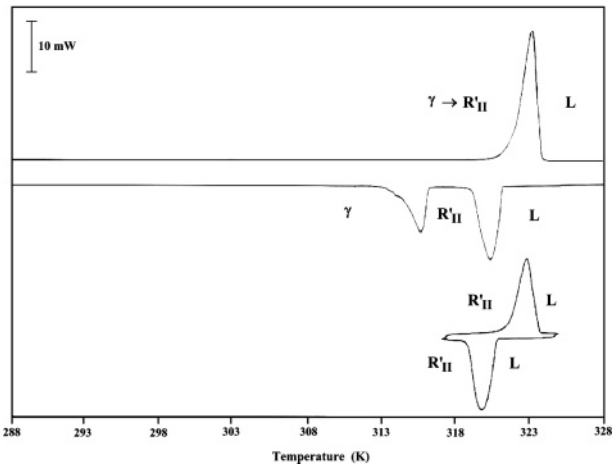

Figure 8. Heating and cooling DSC curves of $C_{16}OH$.

Table 5. γ-Form of $C_{16}OH$: Hydrogen-bonding Parameters

O−H···O′	H···O′ (Å)	O···O′ (Å)	O-H···O′ (°)
$O-H_{O1}\cdots O'$	1.897	2.675	136.15
$O-H_{O2}\cdots O'$	1.882	2.638	133.54

Table 6. Transition Temperatures and Enthalpies of $C_{16}OH$

	$\gamma \rightarrow R'_{II}$		$R'_{II} \rightarrow L$	
C_n	T (K)	ΔH (kJ/mol)	T_m (K)	ΔH_m (kJ/mol)
$C_{16}OH$	321.1 ± 0.5	24.2 ± 1.6	321.6 ± 0.5	33.1 ± 1.3

Concerning intermolecular interactions, since hydrogen bonds lie between both centers of symmetry and 2-fold axes, hydrogen atoms linked to the oxygen ones are presumably distributed randomly over two possible positions, taken with C15−C16−O−H_O torsion angles of 180° and 60° for H_{O1} and H_{O2}, respectively (each with an occupancy factor of 0.5). This disordered distribution of the hydrogen atom had already been reported by Abrahamsson et al., as well as by Fujimoto et al.[56] and Michaud et al.[57] in the cases of octadecanol and eicosanol, respectively. Hydrogen-bonding parameters (bond lengths and angles) are given in Table 5.

For both components (C_{16} and $C_{16}OH$), additional information, including atomic coordinates, detailed bond lengths and angles, and intermolecular contacts, are available elsewhere (see Supporting Information).

Transition temperatures and enthalpies were deduced from DSC analyses. As can be seen in Figure 8, a unique signal is observed on heating, while two signals, corresponding to the crystallization and solid−solid phenomena, are clearly visible on cooling. That means that, on heating, the solid−solid transition is overlapped with the solid−liquid one. Melting temperatures and enthalpies were obtained from a second heating from a temperature above the $R'_{II} \rightarrow \gamma$ transition. Thermo-energetic parameters are given in Table 6. Both transition temperatures are very close to one another. As for C_{16}, the global transition enthalpy is high, which

(56) Fujimoto, K.; Yamamoto, T.; Hara, T. *Rep. Prog. Polym. Phys. Jpn.* **1985**, *28*, 163.
(57) Michaud, F.; Ventolà, L.; Calvet, T.; Cuevas-Diarte, M. A.; Solans, X.; Font-Bardía, M. *Acta Crystallogr.* **2000**, *C56*, 219.

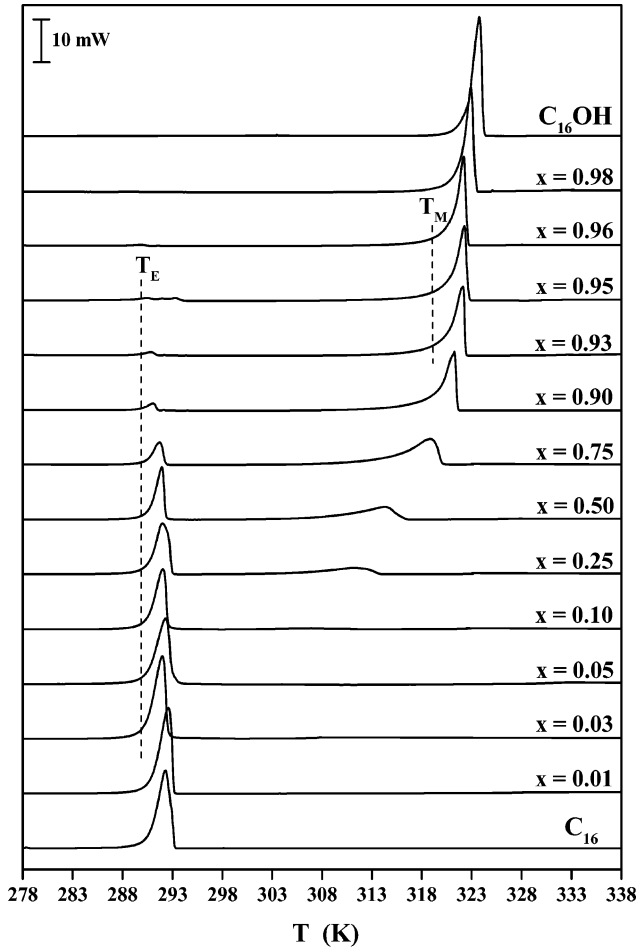

Figure 9. DSC thermograms as a function of molar fraction in $C_{16}OH$.

means that $C_{16}-C_{16}OH$ binary mixtures could be promising energy storing materials.

Phase Diagram Determination. The experimental phase diagram was established by combining DSC and isothermal XRD techniques. Twelve binary mixed samples were analyzed.

Energetic Characterization. Calorimetric measurements led to the determination of phase transitions as well as their temperatures and enthalpies. DSC thermograms, obtained between 278 and 338 K, are given in Figure 9 as a function of molar composition x in $C_{16}OH$. This set of curves clearly reveals the presence of two invariants: (1) a eutectic one, covering a large part of the composition range (approximately from 3% to 93% in $C_{16}OH$) and located around $T = 290$ K. (2) A metatectic one, located around $T = 319$ K for compositions rich in $C_{16}OH$ (approximately from 93% to 96%).

The presence of the eutectic invariant has already been reported in the literature, located at $T = 291.04$ K.[29] On the other hand, these authors have not observed the metatectic one.

Crystallographic Characterization. X-ray diffraction analyses were performed on a Siemens D500 vertical powder diffractometer. Data were collected at $T = 273$ K and $T = 298$ K (i.e., below and above the eutectic invariant temperature) in order to determine the limits of monophasic and biphasic domains, as well as their natures.

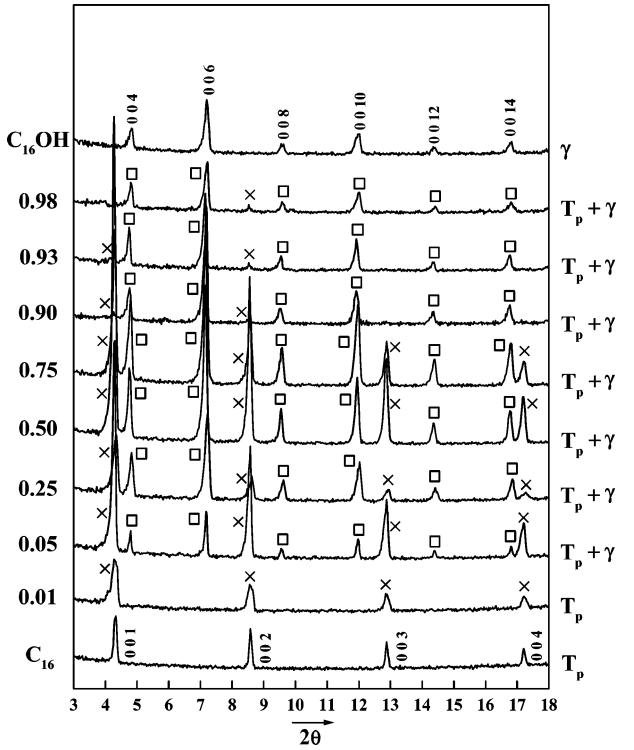

Figure 10. Isothermal X-ray diffraction patterns (00*l* reflections) recorded at $T = 273$ K, as a function of the molar fraction x in $C_{16}OH$. The symbols × and □ correspond to the T_p and γ forms, respectively. Peak intensity disparities are induced by random preferred orientations.

Measurements at $T = 273$ K. X-ray diffraction patterns are given in Figure 10 as a function of molar fraction x in $C_{16}OH$. They are represented in the most relevant 2θ range, between 3° and 18° (corresponding to the (00*l*) reflections). From $x = 0.05$ to $x = 0.98$, diffractograms display two diffraction pattern families, characterizing the coexistence of the T_p and γ forms. The T_p form is visible in the close vicinity of C_{16} while the γ form has not been observed alone, implying a very narrow single-phase domain in the vicinity of $C_{16}OH$ (probably <1% of the composition range).

Measurements at $T = 298$ K. Representative diffraction patterns, in the 2θ range 3°−18°, are given in Figure 11. They point out the coexistence of the γ form with liquid over a large composition range (approximately from 5% to 95%). A narrow γ single-phase domain is observed in the vicinity of $C_{16}OH$.

The Metatectic Region. The upper part of the phase diagram in the vicinity of $C_{16}OH$ has been characterized by X-ray measurements performed each degree from 318 K (i.e., below the metatectic invariant) to the melting temperature. These experiments have pointed out the presence of a small R'_{II} monophasic domain. As an example, for the composition $x = 0.98$, starting from 318 K, the following sequence is observed with increasing temperature (Figure 12): $[\gamma] \rightarrow [\gamma + R'_{II}] \rightarrow [R'_{II}] \rightarrow [R'_{II} + L]$.

Experimental Phase Diagram and Energetic Data. The experimental phase diagram was established by combining structural and thermal analytical data obtained from the pure components and binary mixed samples. It is represented in Figure 13a, together with the most representative X-ray data determined at 273 and 298 K. Eutectic and metatectic areas

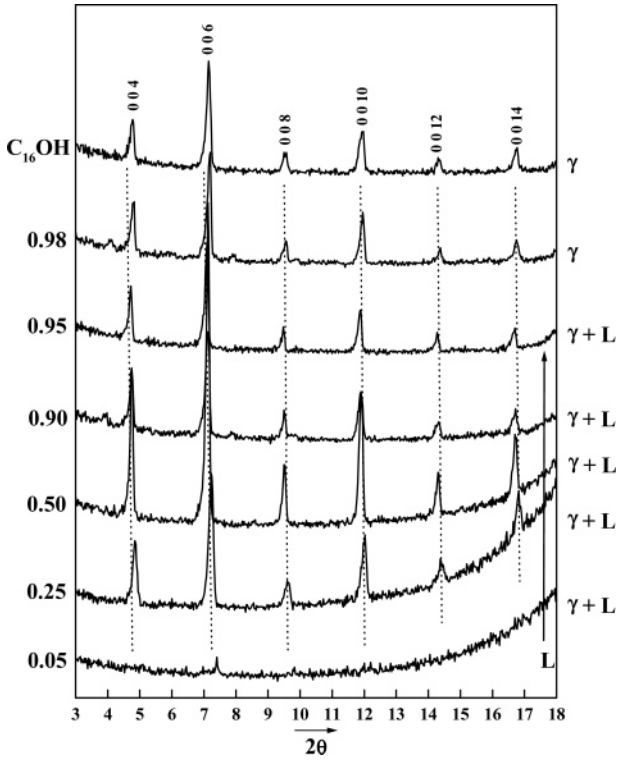

Figure 11. Isothermal X-ray diffraction patterns (00*l* reflections) recorded at $T = 298$ K, as a function of the molar fraction x in $C_{16}OH$.

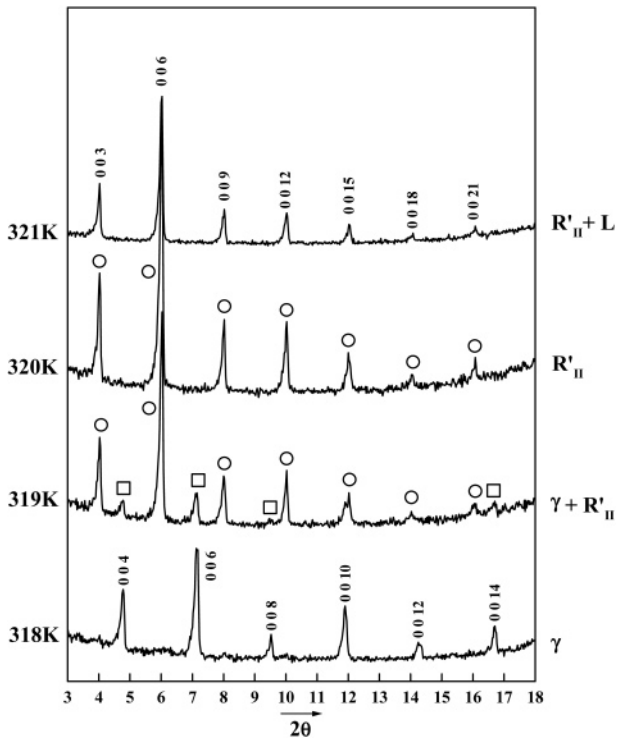

Figure 12. X-ray diffraction patterns (00*l* reflections) of the sample $C_{16}(0.02)C_{16}OH(0.98)$ at $T = 318$, 319, 320, and 321 K. The reflections characterizing the γ and R'_{II} forms are represented by the symbols □ and ○, respectively.

are detailed in Figure 13b. Thermo-energetic data deduced from thermal analyses are given in Table 7.

This diagram exhibits the following:

(1) Four monophasic domains: $[T_p]$, $[\gamma]$, $[R'_{II}]$, and [L]}.

(2) Five biphasic domains {$[T_p + \gamma]$, $[\gamma + R'_{II}]$, $[T_p + L]$, $[\gamma + L]$, and $[R'_{II} + L]$}.

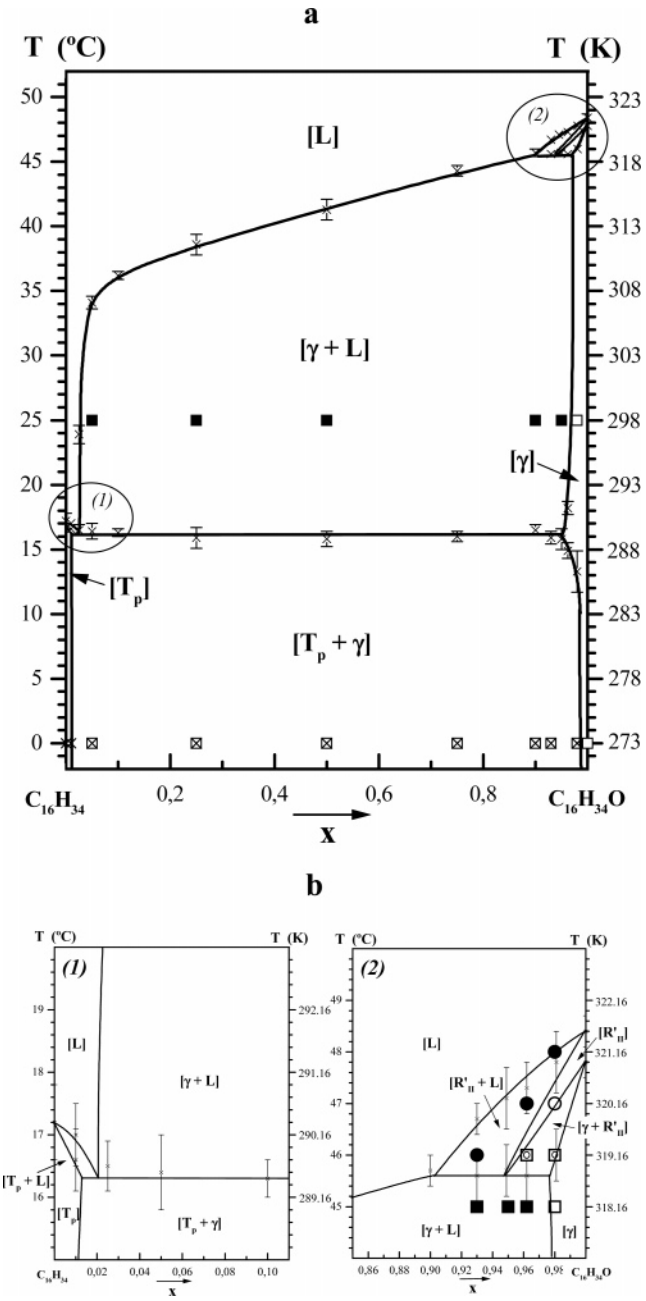

Figure 13. (a) Experimental phase diagram of the $C_{16}-C_{16}OH$ binary system. ×, □, x within a box, and ■ are XRD data corresponding to the $[T_p]$, $[\gamma]$,$[T_p + \gamma]$, and $[\gamma + L]$ phases, respectively. (b) Zooms of the $C_{16}-C_{16}OH$ phase diagram. (1) Eutectic area. (2) Metatectic area. □, ○, ■, and ● are XRD data for the $[\gamma]$, $[R'_{II}]$, $[\gamma + L]$, and $[R'_{II} + L]$ phases, respectively.

(3) Two invariants: (a) a eutectic, located at $T_E \approx 289.5$ K, which covers a large part of the composition range. The Tammann procedure was used to fix the right-hand limit of the latter (Figure 14). The intersection of the straight line with the horizontal axis is found at the molar concentration of $x_2 \approx 0.95$ in $C_{16}OH$. Due to the lack of energetic data in the C_{16} vicinity (the eutectic point being very close to C_{16}), the Tammann procedure did not allow either the determination of the left-hand limit of this invariant or the composition of the eutectic point. Nevertheless, the left-hand limit was estimated to $x_1 \approx 0.012$ and the eutectic point to $x_E \approx 0.02$. (b) A metatectic in the $C_{16}OH$ vicinity, located at $T_M \approx 318.8$ K, between $x_1 \approx 0.905$ and $x_2 \approx 0.975$. The

Table 7. Thermo-energetic Data of the $C_{16}-C_{16}OH$ Mixed Samples[a]

			solid−solid transitions		melting		
x in $C_{16}OH$	T_E	T_M	$T_{[T_p+\gamma\rightarrow\gamma]}$	$T_{solvi[\gamma\rightarrow R'_{II}]}$	T_{sol}	T_{liq}	ΔH_m
C_{16}						290.4 ± 0.6	51.5 ± 1.6
0.01					289.7 ± 0.5	290.2 ± 0.5	51.6 ± 3.4
0.03	289.7 ± 0.4					297.1 ± 0.7	51.1 ± 2.7
0.05	289.6 ± 0.6					307.3 ± 0.5	50.6 ± 3.2
0.10	289.5 ± 0.3					309.4 ± 0.3	53.2 ± 2.8
0.25	289.1 ± 0.8					311.8 ± 0.8	52.2 ± 2.4
0.50	289.0 ± 0.6					314.5 ± 0.8	52.7 ± 2.1
0.75	289.2 ± 0.4					317.5 ± 0.4	51.0 ± 2.0
0.90	289.7 ± 0.4					318.9 ± 0.3	54.9 ± 3.8
0.93	289.1 ± 0.5	318.8 ± 0.5				319.9 ± 0.3	52.8 ± 2.0
0.95	289.0 ± 0.8	318.9 ± 0.5				320.3 ± 0.6	54.2 ± 4.4
0.96		318.8 ± 0.5	288.1 ± 0.6			320.5 ± 0.5	54.5 ± 3.5
0.98			286.5 ± 0.6	319.2 ± 0.5		321.0 ± 0.6	52.8 ± 2.0
$C_{16}OH$				321.1 ± 0.5		321.6 ± 0.5	57.3 ± 2.4

[a] Temperatures are in K and enthalpies in $kJ \cdot mol^{-1}$.

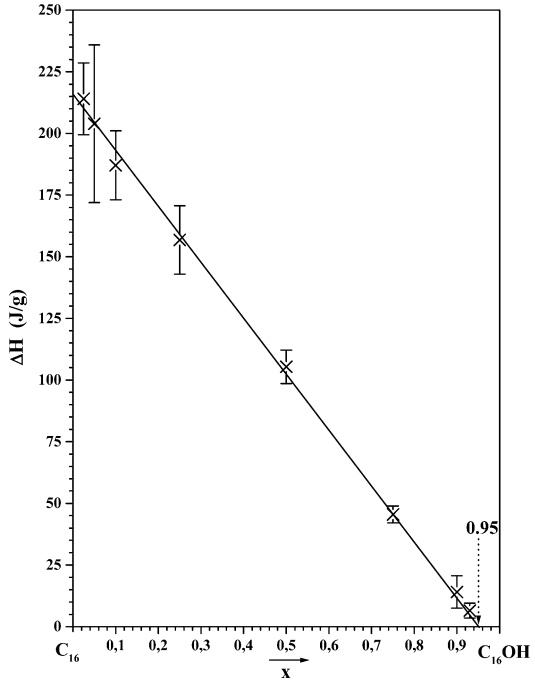

Figure 14. Tammann diagram corresponding to the right-hand side of the eutectic invariant.

molar fraction of the metatectic point was estimated to $x_M \approx 0.95$.

The miscibility in the solid state is very restricted, limited to the regions close to the pure components, whereas the domain of demixion covers a large part of the composition range (approximately 98%).

Application. Due to their high latent heats of melting, these mixed substances are liable to be suitable energy-storing materials, applicable to the thermal protection. To test their efficiency in that particular field, we have extended the study to the design of a container capable of maintaining the temperature of a liquid between 13 and 18 °C as long as possible.

The Container. We have considered a commercial plastic double-wall glass (height: 15 cm; diameter: 8 cm; capacity: 40 cl) originally capable of maintaining, at ambient temperature, a drink around 1 °C for approximately 2 h, by prior solidification in a freezer of the liquid contained within the double wall. The latter (probably water) was removed

Figure 15. Plastic double-wall glass and the measurement system.

to be replaced by a Molecular Alloy Phase Change Material (MAPCM) (Figure 15).

The MAPCM. To maintain the temperature quasi-constant, the required material has to display a narrow thermal window, in association with a suitable melting temperature. Finally, the selected molecular alloy has the following characteristics: Composition: $C_{16}(0.99)C_{16}OH(0.01)$; liquidus temperature: $T_{liq} = 17.0$ °C; thermal window: $l = 0.5$ °C; melting enthalpy: $\Delta H_m = 228$ J/g. For economical matters, we have selected an alloy with a small amount of $C_{16}OH$ (instead of pure C_{16}) since such a material could be commercially available at lower cost.

Principle. Beforehand, to be operational, the glass has to be placed long enough in a fridge to cool and solidify the MAPCM. Then, the glass is removed from the fridge and the desired liquid poured inside. Under the effect of external heat, the MAPCM is heated, its temperature rises, and energy is stored in the sensible heat form, until melting begins at solidus temperature. During the melting process, it stores the energy in the latent heat form, maintaining the liquid inside the glass at quasi-constant temperature (due to the narrow thermal window). When the MAPCM has totally melted (i.e., at liquidus temperature), its temperature rises again and sensible heat storage takes place, until the external temperature is reached. The total process time mainly depends on the external temperature (the higher external

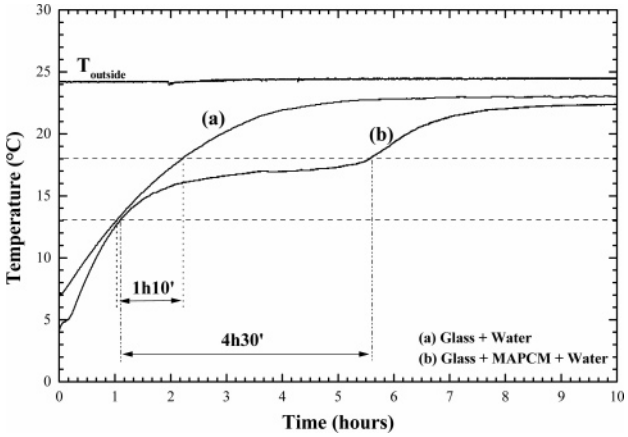

Figure 16. Thermal behaviors of the "active" and "blank" glasses containing water, as a function of time.

temperature means the lower the time) and on the quantity of MAPCM used (the lower mass means the lower the time).

Results. The liquid used for testing the efficiency of the MAPCM is freshwater, previously maintained around 6 °C in a fridge. The thermal behavior of the water in the glass containing the MAPCM ("active" glass) was compared to the one in the same glass without MAPCM ("blank" glass). The quantity of MAPCM within the double wall of the "active" glass is about 230 g. In both cases, glasses containing freshwater were submitted to an external temperature of approximately 24 °C. The temperature within the water was measured as a function of time. The probe was placed in the middle of the glass (Figure 15). Results are plotted in Figure 16. They clearly point out a positive effect of the MAPCM, the water contained in the "active" glass being maintained in the required temperature range (i.e., between 13 and 18 °C) for approximately 4.5 h, which means almost 4 times higher than in the case of the "blank" glass.

In the case of an application requiring a slow-temperature variation through a wide temperature range, one could imagine using $C_{16}-C_{16}OH$ mixed samples involving large thermal windows (i.e., compositions between $x \approx 0.1$ and $x \approx 0.9$ in $C_{16}OH$).

Conclusion

Low-temperature crystal structures of hexadecane and 1-hexadecanol (T_p and γ forms, respectively) have been determined from powder X-ray diffraction data. Despite the similarity of chain lengths, both molecules display significant interaction and structural differences, giving rise to a little miscibility in the solid state between the two components. The experimental phase diagram exhibits eutectic and metatectic invariants with very low solubility in the solid state for alloys rich in C_{16} as well as in $C_{16}OH$ (1−2% of the composition range for T_p and γ alloys and around 5% for R'_{II} alloys). These conclusions are somewhat different from those proposed previously by Plesnar et al., who have pointed out a total immiscibility of the two components in the solid state.[29]

From a practical point of view, resulting alloys can be considered as suitable MAPCMs for applications in the fields of energy storage and thermal protection. Such a material has been used for the design of an "active" double-wall glass capable of maintaining a liquid submitted to an external temperature of 24 °C between 13 and 18 °C for approximately 4.5 h.

In the future, this work will be extended to binary systems involving other organic families, such as carboxylic acids. The study of the two systems between hexadecane ($C_{16}H_{34}$) and palmitic acid ($C_{16}H_{32}O_2$) and hexadecanol ($C_{16}H_{33}OH$) and palmitic acid are already in progress.

Supporting Information Available: Atomic coordinates, bond lengths and angles, torsion angles, and intermolecular contacts for the T_p form of C_{16} and the γ form of $C_{16}OH$ (PDF). This material is available free of charge via the Internet at http://pubs.acs.org.

CM050130C